IEEE Access
Multidisciplinary | Rapid Review | Open Access Journal

Received June 12, 2018, accepted July 20, 2018, date of publication August 1, 2018, date of current version August 20, 2018.

Digital Object Identifier 10.1109/ACCESS.2018.2860795

A Capacitive Coupled Patch Antenna Array With High Gain and Wide Coverage for 5G Smartphone Applications

MANOJ STANLEY[1], YI HUANG[1], (Senior Member, IEEE), HANYANG WANG[2], (Senior Member, IEEE), HAI ZHOU[2], AHMED ALIELDIN[1], AND SUMIN JOSEPH[1]

[1]University of Liverpool, Liverpool L69 3GJ, U.K.
[2]Huawei Technology Co., Ltd., Reading RG2 6UF, U.K.

Corresponding author: Yi Huang (yi.huang@liv.ac.uk)

This work was supported by Huawei Technologies, Shenzhen, China.

ABSTRACT In this paper, a novel capacitive coupled patch antenna array capable of providing high gain and 360° coverage in the elevation plane is proposed. The proposed antenna element is studied in detail using the theory of characteristic modes to enhance the bandwidth. It exhibits a uniform radiation pattern with a stable gain when integrated with the mobile phone chassis. These elements are positioned in the mobile phone chassis as a set of four sub-arrays each with 12 antenna elements to provide high realized gain around 16.5 dBi with each sub-array providing 90° coverage. The antenna array is fabricated, and the beam steering performance of the array is evaluated using a beam-steering test bed. The results show that it covers the frequency range of 24–28 GHz, which is a promising band for future 5G-based smartphone services as predicted and could be a strong candidate for 5G applications.

INDEX TERMS 5G antenna, beam steering, capacitive coupling, mm-wave, patch antenna, phased array, smartphone.

I. INTRODUCTION

In recent years, there has been a shortage of frequency spectrum below 6 GHz bands and the demand for higher data rate is rising. Recent research is focused on developing mm-Wave antenna arrays around 28 GHz for 5G mobile phone applications [1], [2]. In [3], researchers at Samsung America developed a mesh type patch antenna with dual feeds to achieve dual polarization around 28 GHz. But the bandwidth achieved was narrow. The antenna was placed in the plane normal to the PCB as opposed to the conventional PCB plane placement. In [4], notch antennas based on microstrip feeding and aperture coupled slot antennas were employed to design 1 × 4 arrays. The antenna was compact, but the bandwidth achieved was narrow. In [5], antenna design utilizing multi-layer PCB and metal cap was demonstrated with a 2 GHz bandwidth around 28 GHz. The design thickness was 6.5 mm and was too high for implementation in modern mobile phones. In [6], off-center dipole elements were used to obtain a 2 GHz bandwidth around 28 GHz. But the feeding mechanism was complicated and the design had multiple layers. In [7], a 1 × 4 array using curved dipole antenna elements was designed to achieve a high bandwidth. But the achieved gain was around 8 dBi which is not sufficient for practical applications. A wide beam antenna design was implemented in [8] with a bandwidth of 3.9 GHz using substrate integrated waveguide (SIW) technology, but achieved a low gain. A 1 × 4 vertical monopole array was used in [9] to obtain a wide beam coverage, but with a low gain and a narrow bandwidth around 28 GHz. Two different dielectrics were used in this design. In [10], an SIW based slot antenna was integrated with SIW power dividers and phase shifters to generate fixed beams based on Butler matrix principle. The system covered the frequency band 26-30 GHz achieving a bandwidth of 4 GHz. But the overall size of the system was 72 mm × 27.4 mm × 0.54 mm which almost occupied a quarter of the mobile phone's area and is too large for practical implementation. In [11], a 3D array configuration was proposed with a probe-fed patch antenna as an antenna element. The array was capable of covering 270° in the azimuth plane. But the bandwidth of the patch antenna was too narrow.

In [12], a loop-slot antenna was proposed and integrated as a 10-element array. The antenna was compact but had strong back radiation and a narrow bandwidth. In [13], Stanley *et al.* proposed a wide bandwidth PIFA antenna with a defected ground structure. However, the design had back radiation due to the defected ground structure. An antenna design to achieve a large bandwidth, high gain, small size and wide beam width simultaneously is a challenging task. Considering these requirements, Stanley *et al.* proposed a capacitive fed patch antenna element in [14] and used this antenna element for a new array configuration for wide coverage. Based on this initial reported work, a comprehensive study of the capacitive fed patch antenna and the array configuration, its practical implementation and testing is reported in this paper. This work includes the bandwidth enhancement, extracting current modes using the Theory of Characteristic Modes and the antenna design parameter study. The antenna array has been fabricated and its beam steering performance is evaluated using a beam steering setup inside the anechoic chamber.

In Section II, the proposed antenna element design and its operation principle are explained using an equivalent circuit model and the Theory of Characteristic Modes. The effect of critical design parameters on antenna element performance is also discussed in this section. The antenna array architecture, design and performance are described in Section III. The measurement setup to evaluate the beam steering performance of a 1 × 4 array is also discussed in section III. A modified design to widen the bandwidth is presented in Section IV. The antenna array is compared with the state-of-the-art antenna array designs in Section V. Conclusions are drawn in Section VI highlighting the achievements of this research and future work directions.

II. ANTENNA DESIGN AND PERFORMANCE

A. ANTENNA DESIGN

The proposed antenna is a pair of compact capacitive coupled symmetric patches as shown in Fig. 1. The overall size of the proposed design is 3.7 mm × 3.25 mm. Rogers RT5880 of a relative dielectric constant 2.2 and loss tangent 0.0009 at the frequency band of 24-28 GHz is used as the substrate for printed circuit board (PCB). The patches are printed at the top layer of the substrate. The bottom layer of the substrate consists of the ground plane. The inner conductor of the coaxial probe feed extends from the ground plane through the PCB substrate to reach the top layer feed which capacitively couples the patches.

The antenna element covers 24-28 GHz which is a prospective frequency band for future 5G smartphone applications. The capacitive feed helps to reduce the effective patch size. The width of the patch is $\sim 0.42\lambda_{eff}$ at 26 GHz where λ_{eff} is the effective wavelength in the medium. This reduction in size is due to the capacitive feeding. The parasitic patch improves the impedance bandwidth for 10 dB return loss compared to a single patch antenna.

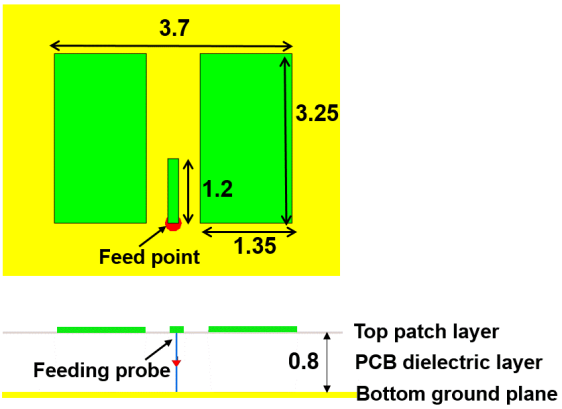

FIGURE 1. Proposed antenna element design (All dimensions are in mm).

B. PRINCIPLE OF OPERATION

Two reference designs are used to demonstrate the working principle of the design. In the first reference design, the feed is done by capacitive coupling, but only one of the patches is used. The resonance occurs around 26 GHz indicating a reduction in resonant frequency from the directly fed patch antenna case which is the second reference design. The resonance occurs around 30 GHz as seen in Fig. 2. The bandwidth for both cases is smaller than the required bandwidth of 4 GHz. In the proposed design, a parasitic patch is added which improves the bandwidth. The direct fed patch antenna has VSWR < 2 over 28.5-30.5 GHz at which 28.5-29.5 GHz is capacitive and 29.5-30.5 GHz is inductive in nature as seen in the Smith chart in Fig 2. The direct fed patch antenna changes from inductive to capacitive at 26 GHz and from capacitive to inductive at 29.5 GHz. In the case of single patch antenna with coupled feed, VSWR < 2 over 25.5-28 GHz at which 25.5-26.75 GHz is inductive and 26.75-28 GHz is capacitive in nature. The proposed design has VSWR < 2 over 24-28 GHz at which 24-26 GHz is inductive and 26-28 GHz is capacitive. The antenna bandwidth is related to the Quality factor or Q factor. The lower the Q factor, the higher the antenna bandwidth is. The Q factor of an antenna is related to the radius of the smallest sphere that encloses the physical structure [15]. The Q factor approaches a lower value when the smallest sphere that can enclose the antenna has a larger radius. For the proposed design, the antenna area increases when an additional patch has been added. This would increase the radius of the smallest sphere that could enclose the antenna structure and reduce the Q factor and hence broaden the antenna bandwidth. This improves the impedance matching over a broader bandwidth when an additional patch is added. The proposed design has resonance behavior similar to the single patch case with a coupled feed, but has a wider bandwidth.

C. EQUIVALENT CIRCUIT MODEL

The equivalent circuit of each of the reference designs along with the proposed design is studied. As seen in Fig. 3(a),

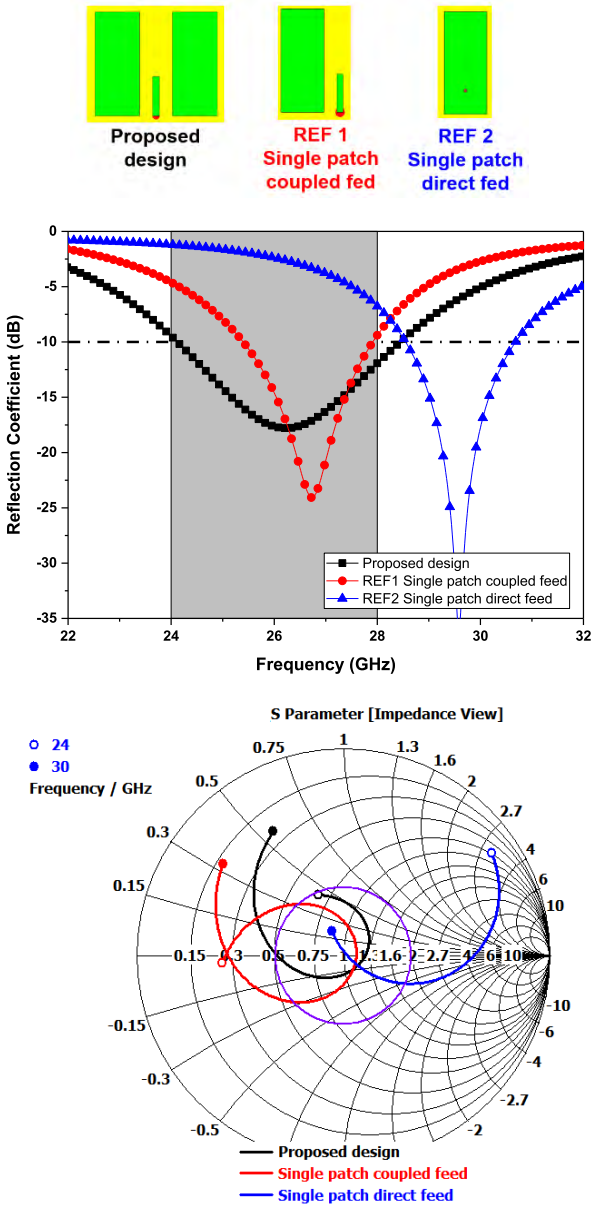

FIGURE 2. Simulated reflection coefficients and impedance loci for reference antennas.

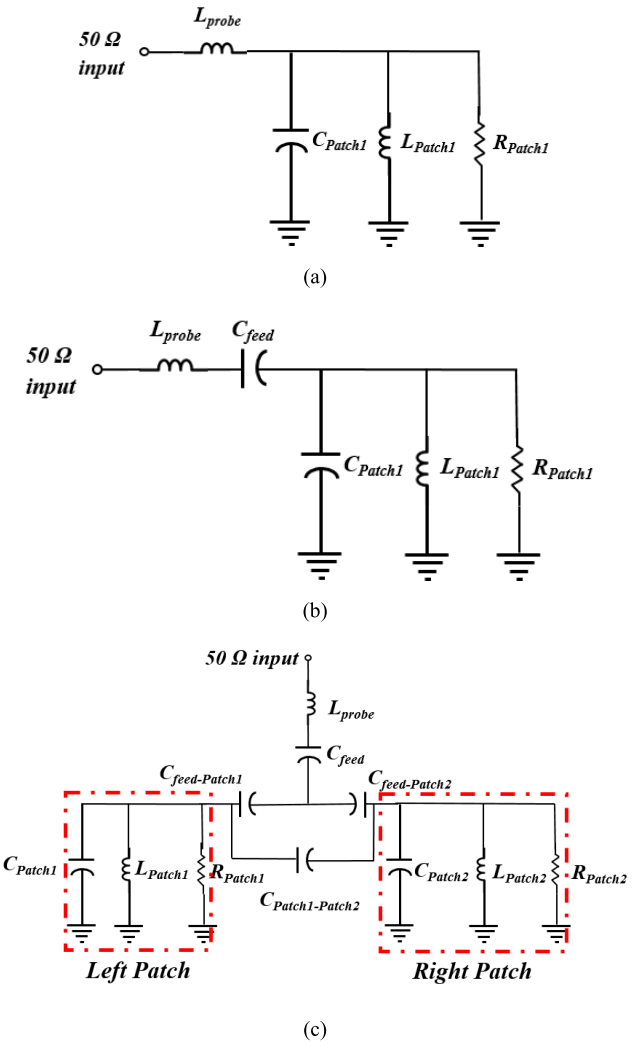

FIGURE 3. Equivalent circuit (a) Single patch direct fed REF2; (b) Single patch coupled fed REF1; (c) Proposed design.

the direct fed patch antenna can be modelled as a parallel resonant circuit in series with the probe inductance [16]. As the probe feed is shifted from the edge of the patch towards the center, the inductance of the patch, L_{Patch1}, is increased and the real part reduces as a function of $cos^2\pi xL$ where x is the distance of the feed from the edge of the patch and L is the effective patch length. The probe inductance becomes significant for thick substrates ($h > 0.02\lambda_0$). This series inductance is cancelled by using capacitive feeding in REF 1 and this can be modelled as additional series capacitance as shown in Fig 3(b). This capacitance can be increased by reducing the length and width of the feed section. The detailed equivalent circuit of the proposed design is shown in Fig. 3(c). Each patch can be represented by the parallel RLC circuit and the parameters are the same for both patches as the dimensions are the same and the patch equivalent circuit is parallel to each other. The feed can be modelled as the same feed circuit as in Fig. 3(b) with probe inductance in series with the feed capacitance which decreases as the feed length/width is reduced. There also exist coupling capacitances $C_{feed-Patch1}$ and $C_{feed-Patch2}$ between the feed and the left patch and right patch. As the feed is shifted from the center towards the right patch, the gap between the feed and the right patch is reduced and so $C_{feed-Patch2}$ is increased. Consequently, $C_{feed-Patch1}$ gets reduced. There also exist a capacitance between the two patches which is represented by $C_{Patch1-Patch2}$ which depends on the gap between the two patches. As the gap increases, the series capacitance decreases around lower frequencies as seen in later section.

D. CHARACTERISTIC MODE ANALYSIS

Recently, the Theory of Characteristic Modes (TCM) [17], [18] has drawn an increased interest in mobile handset

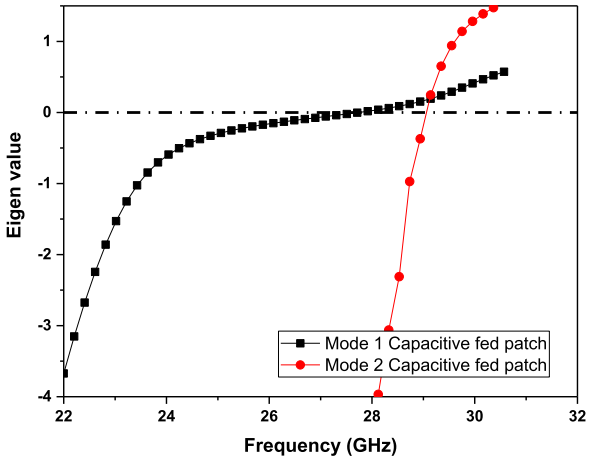

FIGURE 4. Eigen value of characteristic modes of proposed design structure.

antenna design. TCM brings clearer insights into the physical behavior of an antenna, by providing a framework for analyzing the antenna structure independent of the feeding arrangement by identifying the natural Eigen modes (characteristic modes) of a scatterer.

The generalized Eigen value equation is given by,

$$X\left(J_n\right) = \lambda_n R(J_n) \tag{1}$$

where X and R are the imaginary and real parts of an impedance matrix Z which is obtained from the electric field integral equation (EFIE), as derived in [17]. J_n denotes the characteristic mode current of n-th mode on the structure, and λ_n is the corresponding Eigen value. A mode n is resonant at the frequency at which λ_n equals zero. The total current on a conductive surface excited by the feed can be expressed as a linear superposition of the normalized characteristic mode currents as

$$J = \sum \alpha_n J_n \tag{2}$$

where α_n is the modal weighting coefficient of the n-th mode and represents the contribution of the corresponding mode to the total antenna surface current.

The Eigen value of characteristic modes of proposed design without excitation is shown in Fig 4 which indicates that two characteristic modes are present within the frequency range of 22-32 GHz. The corresponding characteristic mode currents of each mode at its resonant frequency is shown in Fig 5. In mode 1, strong vertical currents can be seen in both of the patches in the same direction as the feed patch current direction at 24 GHz. At 28 GHz, the currents in the patches are in the opposite direction as the feed patch section. This phase reversal at 28 GHz is due to the parasitic capacitances between the feed section and the patches which become dominant at higher frequencies. Strong currents exist in the middle patch section from 24-28 GHz for mode 1. The vertical currents are the strongest when the length of the longer side of the patch becomes comparable to $0.4\lambda_{eff}$.

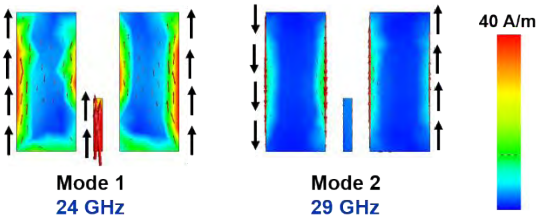

FIGURE 5. Characteristic mode currents of proposed design structure.

The currents on the ground plane are in the opposite direction as on the top patches because of the coupling between the patch and the ground plane. It is recommended that the length of the shorter side of the patch be less than $0.4\lambda_{eff}$ to avoid exciting horizontal mode so as to minimize the distortion of the radiation pattern. In this design, the length of the shorter edge is kept less than $0.2\lambda_{eff}$ to suppress the horizontal mode within the frequency band of 24-28 GHz. In mode 2, strong anti-parallel vertical currents can be seen on the patches at 29 GHz. This mode resonates at a higher frequency because there is no capacitances between the feed and the patches as the fields are cancelled due to the anti-parallel currents. There is no current on the middle patch section. The radiation pattern of each mode at its resonant frequency is shown in Fig.6. Mode 1 has a broadside pattern as the currents on the patches are in phase and the fields add together constructively. In mode 2, the currents on the patches are opposite to each other and hence cancel out the radiation in the broadside direction in mode 2. Combining both modes can improve the coverage, but at additional complexity. Fig. 6 shows the radiation pattern for the patch modes without considering the effect of the ground plane. The mobile phone ground plane size is electrically large compared with the patch structure modes and hence the ground plane modes do not affect the patch modes. When the ground plane is added to the structure, it acts as a reflector and the back radiation will be significantly minimized.

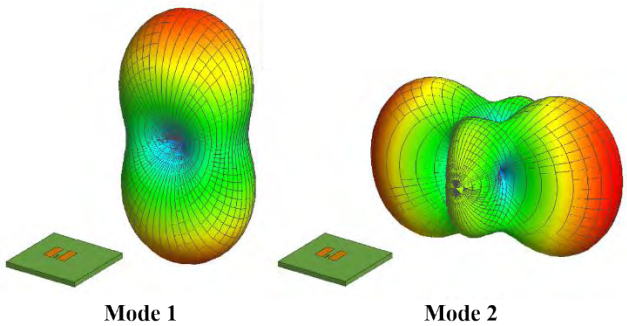

FIGURE 6. Radiation pattern of Eigen modes at resonant frequency.

For our operation, broadside radiation pattern is desired and hence mode 1 is desired and mode 2 is to be eliminated. Mode 1 can be selected by exciting the structure at maximum mode 1 Eigen current location and mode 2 can

be suppressed by placing the feed at weak mode 2 Eigen current location. In this structure, the middle patch section acts as a suitable feed location to excite mode 1 and suppress mode 2. There is a slight shift in the resonant frequency from 28 GHz as predicted using TCM to 26 GHz upon excitation. The total current distribution is simulated in CST Microwave Studio with the excitation in the middle of the patches. The total current distribution on the structure at 24 GHz and 28 GHz with excitation is due to mode 1 currents as seen in Fig. 7(a) and Fig. 7(b).

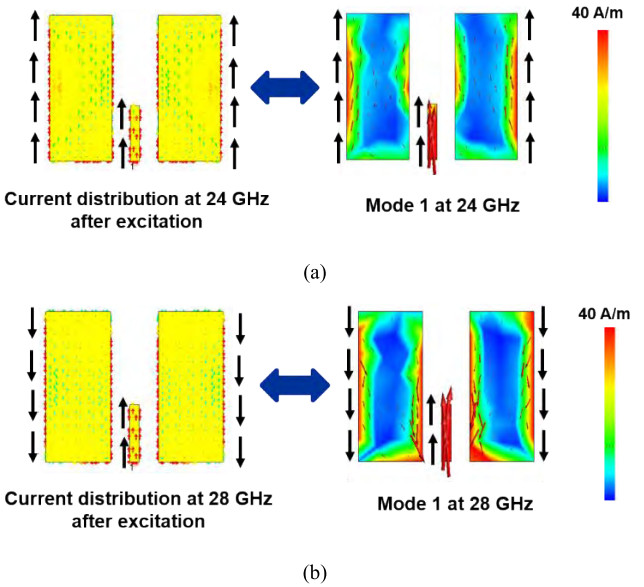

FIGURE 7. Comparison of current distribution after excitation with modal currents at (a) 24 GHz; (b) 28 GHz.

E. ANTENNA ELEMENT PERFORMANCE

The proposed antenna design has 10 dB return loss over the frequency band of 24-28 GHz which means a bandwidth of 4 GHz. The antenna has a total efficiency greater than 90% throughout 24-28 GHz. The antenna element has been fabricated on a Rogers RT5880 board and tested. The antenna is fed using a 50 Ω SMPM male connector which has low loss up to 40 GHz. An SMPM female to a K male cable is used to connect the antenna feed to a vector network analyzer. It can be seen in Fig. 8 that the measured reflection coefficient agrees well with the simulated results. The antenna has a stable gain and uniform broadside radiation pattern throughout the band of interest with a gain greater than 6.26 dBi as shown in Fig 9.

For radiation pattern measurement of the single antenna element, the transmit antenna (a standard horn) and the antenna under test (AUT) are connected to the two ports of the VNA as shown in Fig. 10(a) and the AUT is rotated in steps. The measured and simulated radiation patterns of the antenna element are shown in Fig. 10(b) and show close agreement. A strong radiation can be seen at the boresight as expected. The measured gain is close to the simulated gain as seen in Fig. 11 and is better than 7.4 dBi from

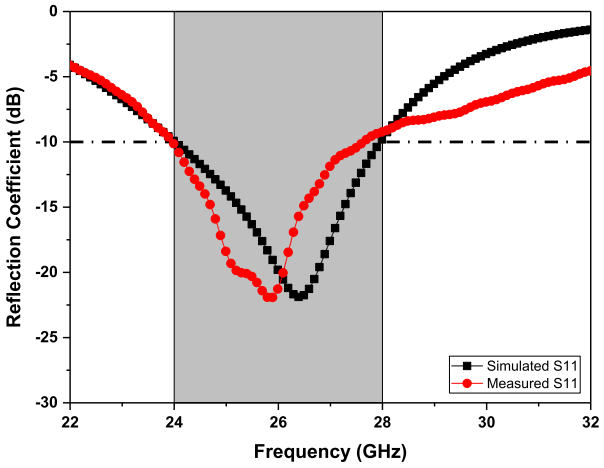

FIGURE 8. Measured & simulated reflection coefficient of the antenna element.

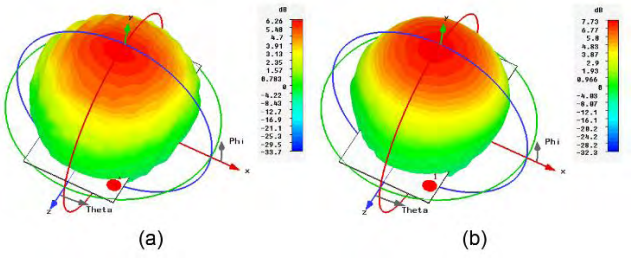

FIGURE 9. Simulated 3D radiation pattern of antenna element in mobile phone chassis (a) 24 GHz; (b) 28 GHz.

26.5-28 GHz at boresight. The slight difference between the simulated and measured realized gains at 26 GHz is possibly due to the SMPM connector. The simulated realized gain for direct fed patch antenna sharply decreases from its resonance frequency at 30 GHz. The coupled feed single patch antenna exhibits a lower realized gain compared with the proposed antenna element because of the reduced effective antenna aperture. For the gain measurement, first, the $S21_{REF}$ between a transmit antenna and a reference antenna with known gain is measured. Then $S21_{AUT}$ between the transmit antenna and the AUT is measured. After these steps, post-processing is done to calculate the realized gain of the AUT. The transmit antenna works only from 26.5-40 GHz. Hence the gain measurement was done only from 26.5 GHz using the equation below to obtain the gain of the AUT.

$$\text{Gain}_{\text{AUT (dBi)}} = \text{Gain}_{\text{REF antenna (dBi)}} + [S21_{AUT} - S21_{REF}] \quad (3)$$

Two identical standard gain mm-wave horn antennas were used as the transmit antenna and the reference antenna.

F. DESIGN PARAMETER STUDY

It is necessary to understand how the design parameters affect antenna performance. To optimize the antenna performance, some important design parameters and their effects are studied.

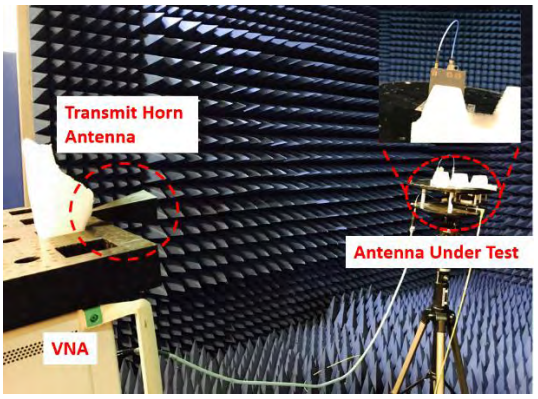

(a)

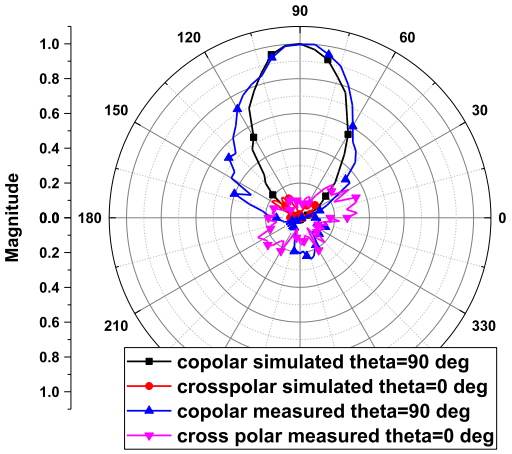

(b)

FIGURE 10. (a) Measurement setup for radiation pattern of the antenna element; (b) Measured and simulated radiation pattern of the antenna element at 26 GHz.

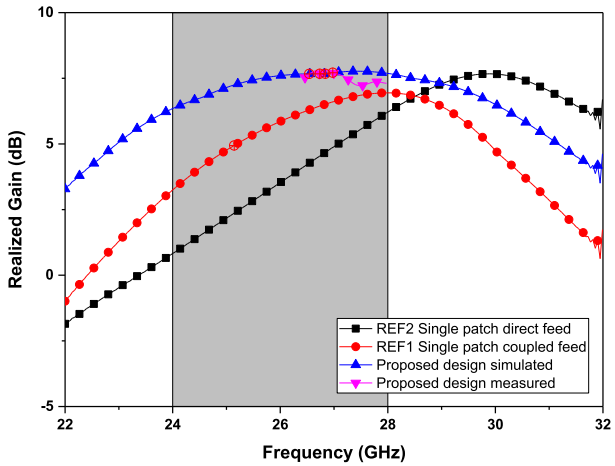

FIGURE 11. Comparison of measured and simulated realized gain of the proposed antenna element with simulated reference antenna realized gain.

The most important parameter of the antenna design is the width of the patch. The patch width controls the resonance around 28 GHz. As the patch width increases, the resonant frequency decreases. This can be seen in Fig 12. The variation of resonant frequency with patch width also proves that the antenna is indeed capacitive coupled patch and not a capacitive coupled dipole antenna.

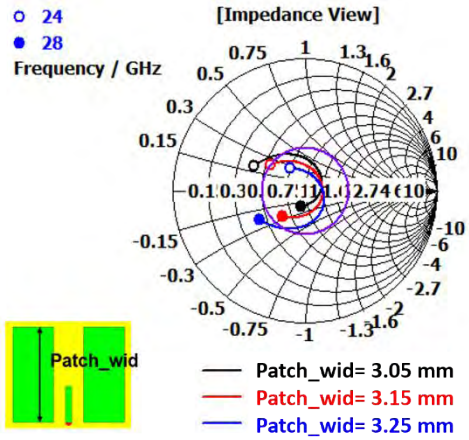

FIGURE 12. Variation of reflection coefficient with patch width.

The patch length can be used as an additional parameter for impedance matching. There is no significant shift in resonant frequency with change in overall patch length, but a minor variation at higher frequencies around 28 GHz. However, if the length of the short side of one of the patches is increased such that the length becomes comparable to $0.4\lambda_0$, horizontal mode of the patch will be excited. Although exciting this mode can generate a wider bandwidth, it will adversely affect the orientation of the radiation pattern and the polarization.

The patch gap folds the impedance loci around 24 GHz as seen in Fig 13. There is no significant variation around upper-frequency range. This parameter can also be used for impedance matching.

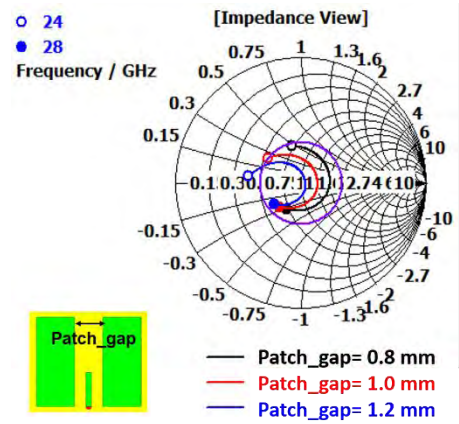

FIGURE 13. Variation of reflection coefficient with patch gap.

The feed length controls the series capacitance as seen in Fig 14. As the feed length decreases, series capacitance of the antenna decreases. The corresponding change in reflection coefficient plot is drastic. Hence this is a critical

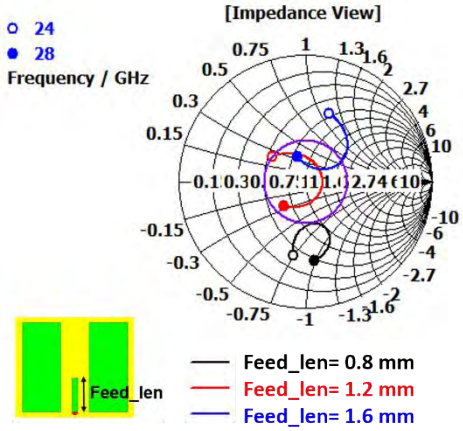

FIGURE 14. Variation of reflection coefficient with feed length.

parameter that needs attention during fabrication. This trend is the same throughout the frequency range.

III. ARRAY DESIGN AND PERFORMANCE

A. ARRAY ARCHITECTURE

The antenna array architecture is described in this section. Fig. 15 describes the methodology to integrate the mm-Wave 5G antenna module inside the mobile phone [19]. The feeding mechanism integrates the antenna elements as a part of the main PCB where the RFIC uses an RF phase shifter to provide progressive phase shifts to each antenna element to implement array scanning [20]. By integrating the antenna element as part of the PCB, cost of production and the height profile can be significantly reduced. The feed line from the RFIC to the antenna element has been modelled as a discrete port in CST MWS simulation. A block diagram of one sub-array is shown in Fig. 16. One sub-array consists of 12 antenna elements each of which is connected to the RFIC. Each of the RFIC is powered using the DC lines from the digital IC [21].

B. ARRAY DESIGN

The mobile phone chassis is modified to accommodate the antenna arrays [11], [14]. In this work, the mobile phone PCB is reshaped from a flat PCB to a 3D shaped PCB. This is a futuristic approach and does not conform to the norms of the existing mobile phone PCB. The 3D-shaped PCB utilizes the thickness of the whole mobile phone which is typically 7-9 mm and can also provide mechanical support for the mobile phone (like a casing). By evolving the shape from flat to 3D, more space for placing the components in the PCB can be obtained, especially for the additional 5G antenna elements along with its corresponding RFIC. The three-dimensional antenna array configurations with the capacitively coupled patch antenna integrated with the mobile phone chassis is shown in Fig. 17.

The proposed arrangement consists of four sub-arrays with three sub-arrays of proposed antenna elements on different

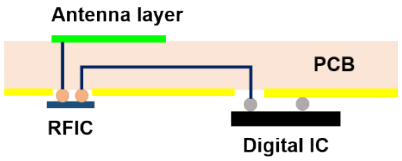

FIGURE 15. Antenna element feeding scheme [19].

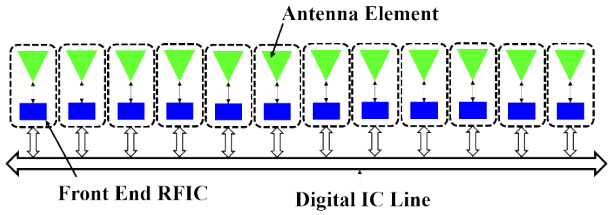

FIGURE 16. Block diagram of one sub-array [21].

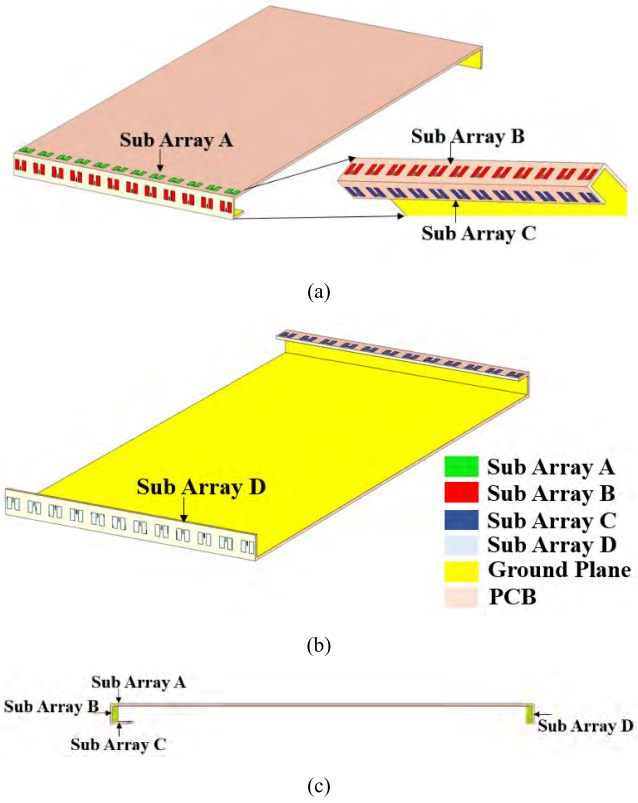

FIGURE 17. Proposed antenna design and array configuration (a) Perspective view of mobile phone PCB; (b) Flipped image of PCB; (c) Side view of PCB.

sides of the bottom edge region in PCB and one sub-array at the sides of the top edge region in PCB. The antenna elements are spaced at a distance of 6.3 mm which is close to $\lambda/2$ at 24 GHz to ensure adequate isolation. Each sub-array has 12 antenna elements and 48 antenna elements are used altogether. Each sub-array provides 90° coverage in the theta plane. Hence the four sub-arrays altogether cover the

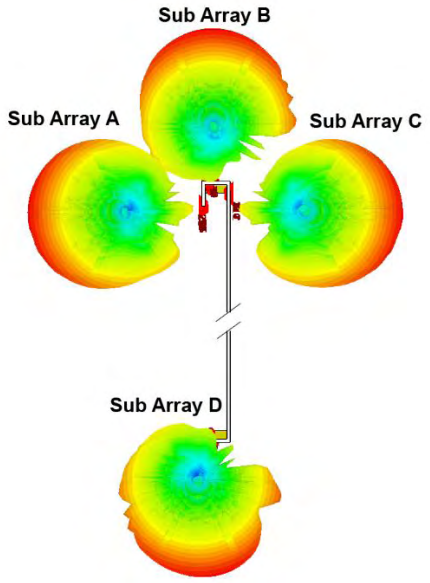

FIGURE 18. Radiation pattern of sub-arrays providing 360° coverage.

entire 360° in the theta plane as shown in Fig. 18. In the phi plane, the 3 dB beam-width is very narrow and not sufficient to cover the remaining phi plane. Beam steering can be utilized in that case using array scanning to steer the beams from −60° to 60° in the phi plane.

C. ARRAY PERFORMANCE

The antenna array covers the frequency range of 24-28 GHz as shown in Fig. 19. Here A1, B1, C1, and D1 represent the first element of sub-array A, sub-array B, sub-array C and sub-array D respectively. A2 represents the second element of sub-array A. The worst-case isolation is around 16 dB between two adjacent antenna elements within sub-array A. This can be improved by increasing the spacing between the antenna elements. The worst case isolation performance

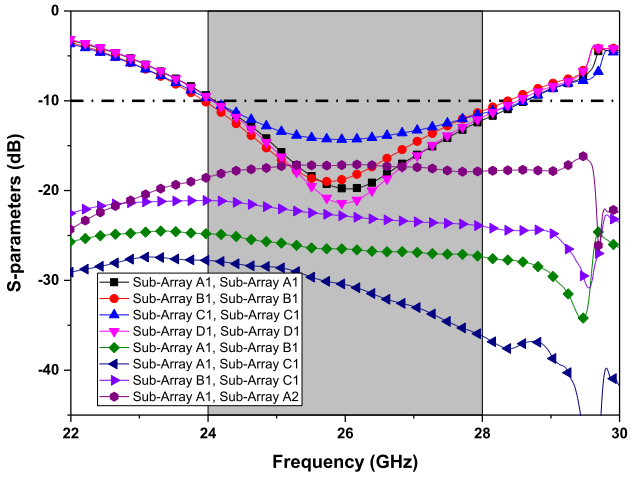

FIGURE 19. Simulated reflection coefficient of the antenna array.

satisfies industrial requirement without need for additional decoupling structures. However, the isolation can be further improved by reducing the magnetic coupling using wave trapping structures [22]. Although, these techniques, improve the isolation by storing some magnetic energy in the wave trapping structure, isolation is improved at the expense of overall realized gain. The worst-case isolation between two elements in the adjacent arrays is around 21 dB for sub-array B and sub-array C. The antenna has a total efficiency greater than 85% throughout 24-28 GHz.

The peak realized array gain at boresight is around 16.5 dBi for each sub-array and the pattern beamwidth is around 8.8° in the phi plane and 90° in the theta plane. The antenna array scanning was simulated using CST MWS. The signal was fed to a 12-way power divider for each sub-array. It was then fed to an individual phase shifter for each antenna element of each sub-array where various phase progression was made to enable beam steering. The phase shifter output was finally connected to the antenna array. Various phase progressions of 0°, 100° and 200° are provided to generate the steered radiation pattern at 0°, 30° and 60°. The pattern can be steered in the phi plane from −60° to 60° using suitable phase shift to each element as shown in Fig.20.

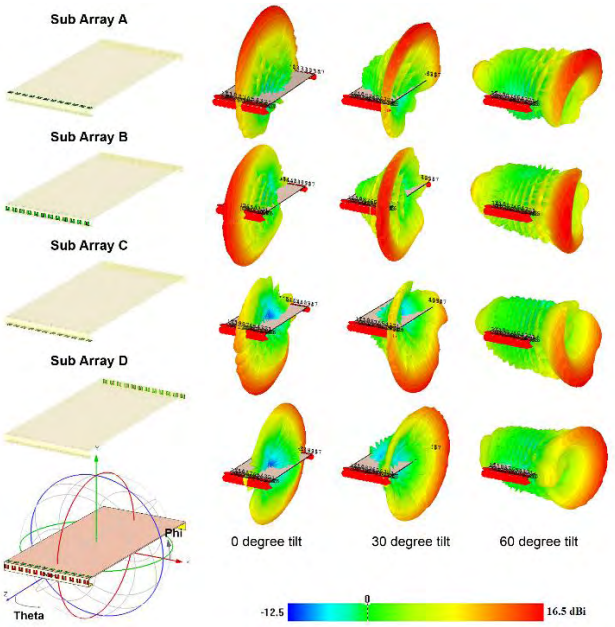

FIGURE 20. Array pattern of 4 sub arrays at different steering angles.

The 3D-shaped PCB can be made possible by separately fabricating the folded section and then finally fusing them together by soldering or aerolite glue. In the future, as the 3D printing technology becomes more matured and supports different substrates, this 3D structure could be fabricated as a single piece. The fabricated prototype is shown in Fig. 21.

The fabricated antenna array has been tested for beam-steering performance. Due to the limited available power divider and phase shifters, only a 1 × 4 antenna array in the sub array D has been tested. The beam steering setup for

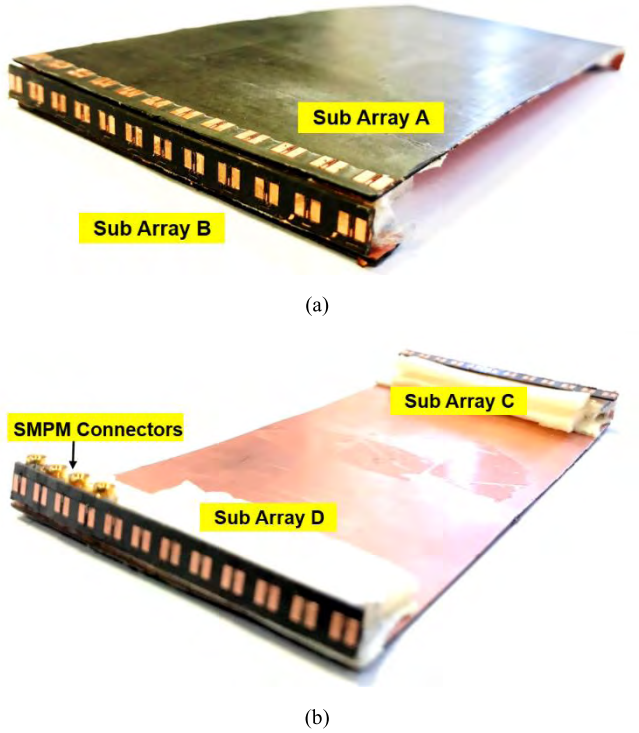

FIGURE 21. Fabricated antenna array (a) Top portion (b) Bottom portion.

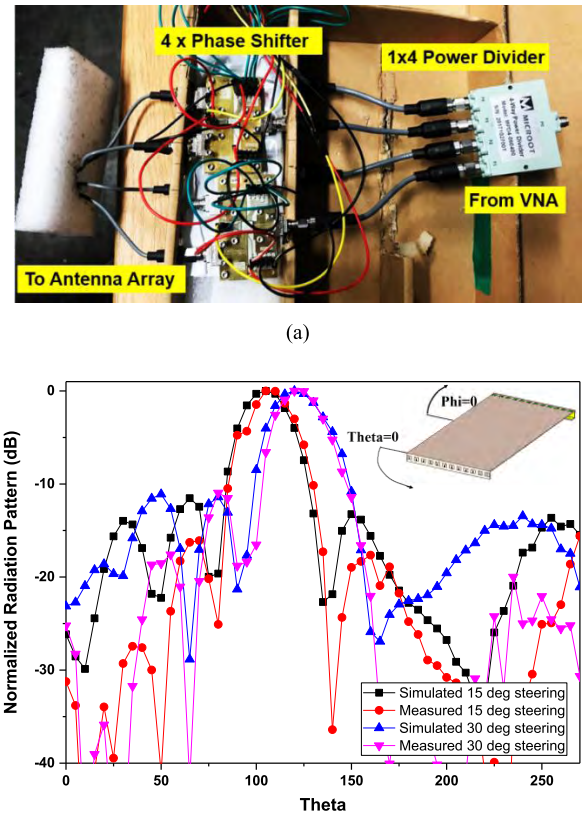

FIGURE 22. (a) Beam steering setup (b) Measured steered radiation pattern of 1 × 4 antenna array for sub array D at Phi = 90.

a 1 × 4 antenna array is shown in Fig. 22 (a). The signal from the VNA is fed to the 1 × 4 power divider module from Microot which operates from 6 to 40 GHz. The outputs of the power divider are connected to the phase shifter modules through 2.92 mm male to 2.92 mm male cables. Different phase states of the digital phase shifter could be varied by programming the digital pins of the phase shifter module using a microcontroller. The phase shifter offers a resolution of 11.25°. The outputs from the phase shifters are fed to the antenna elements of the antenna array using 2.92 mm male cable to SMPM female cables. A SMPM male connector is soldered to the antenna element at the antenna side to make the connection. 4 antenna elements of sub-array D have been tested in this case for beam steering at 15° and 30° from the boresight by supplying a progressive phase shifts of 50° and 100° to the phase shifters respectively. The normalized radiation pattern for different beam-steering angles is shown in Fig. 22 (b). Measured and simulated beamforming results show very good agreements.

As depicted in Fig. 23(b), the simulated realized gain have been studied for the 1 × 12 antenna array in the presence of battery, speaker, microphone, USB connector and LCD screen as shown in Fig. 23(a). A polycarbonate material of dielectric constant of 2.8 has been used as the plastic casing for the mobile phone. As seen from the study, there is a slight reduction in the realized gain which is mostly due to the dielectric losses in the plastic casing. The components are shielded by the ground plane beneath the antenna element for all the sub arrays, thereby, reducing the back radiation to the mobile phone components. The cellular 4G antenna could be positioned along one of the longer edge as a metal strip antenna as proposed in [23]. The GPS and Wi-Fi antennas could also be integrated into the side frame and positioned along the other longer edge as used in [24] without having any conflict with the proposed 5G antenna arrays. The 4G antenna, GPS and Wi-Fi antennas do not affect the performance of the 5G antennas as the electrical separation between them would be greater than 0.5λ at 24 GHz.

IV. BANDWIDTH ENHANCEMENT

The proposed antenna element has been modified to improve the bandwidth. This improved bandwidth comes at the expense of a larger patch. However, this additional bandwidth can be used to counteract the fabrication errors and provide additional flexibility to the design. The modified antenna is a pair of compact capacitive coupled asymmetric patches as shown in Fig. 24. The overall size of the proposed design is 4.8 mm × 3.25 mm. Rogers RT5880 of a relative dielectric constant 2.2 and loss tangent 0.0009 is used as the substrate for printed circuit board of height 0.8 mm.

The modified antenna design has 10 dB return loss over the frequency band of 23.2-30.5 GHz, thereby, having a bandwidth of 7.3 GHz as shown in Fig.25. The antenna has a

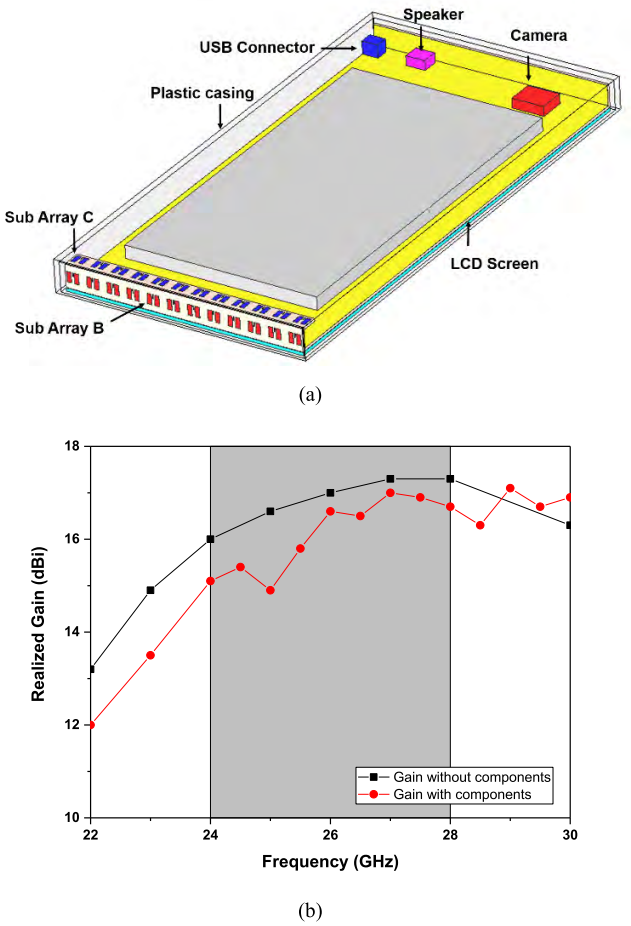

FIGURE 23. (a) Placement of mobile phone components (b) Comparison of simulated realized gain of 12 element antenna array with and without mobile phone components at boresight (sub array D).

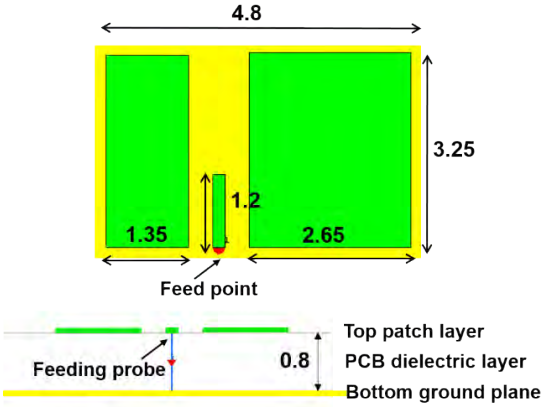

FIGURE 24. Bandwidth enhanced capacitive coupled asymmetric patch antenna.

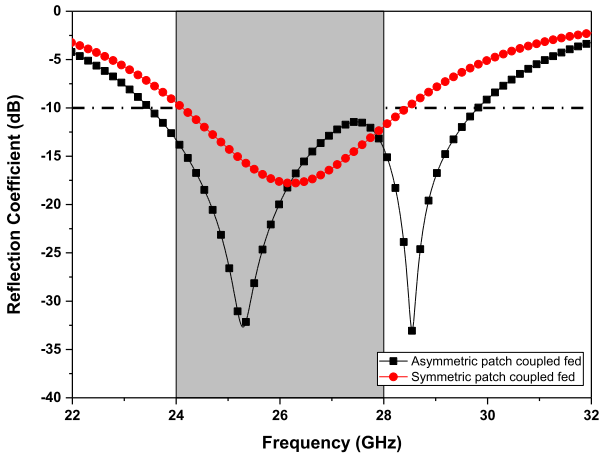

FIGURE 25. Reflection coefficient of asymmetric vs symmetric capacitive coupled patch antenna.

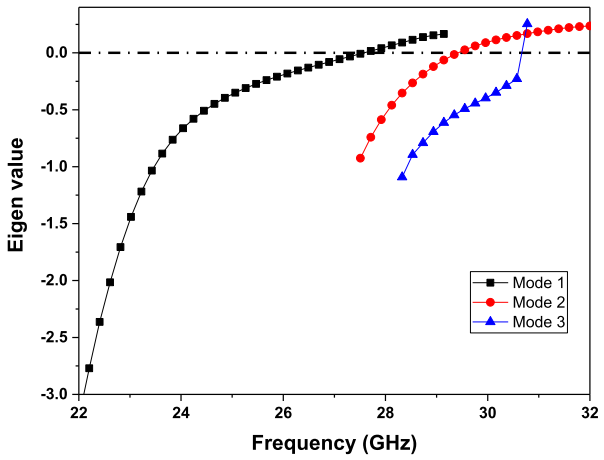

FIGURE 26. Eigen value of characteristics modes of capacitive coupled asymmetric patch structure.

total efficiency greater than 90% throughout 23.2-30.5 GHz and above 95% from 24-28 GHz. The modified antenna has a higher gain than the proposed symmetric patch because of the larger effective area.

TCM simulations have been performed in CADFEKO and the Eigen values of three characteristic modes of the modified design without excitation are shown in Fig 26. In mode 1, strong vertical currents can be seen on the smaller patch and weak diagonal currents on the larger patch at 27 GHz as seen in Fig. 27 and the currents on the ground plane are in the opposite direction as in the top patch because of coupling. The currents on the patches are in the same direction as the strong middle patch current direction. The vertical currents are strongest when the length of the longer side of the patch becomes comparable to $0.4\lambda_{eff}$. The radiation of this mode is mainly due to the vertical mode of the patch. Mode 2 exists from 27-32 GHz. In mode 2, strong anti-parallel vertical currents can be seen on the smaller patch and the larger patch edges at 29 GHz. There is no current in the middle patch section.

Mode 3 exists over 28-30.5 GHz as seen in the Eigen value curve. In mode 3, weak vertical currents can be seen on the smaller patch and strong diagonal currents on the larger patch in a direction opposite to that of the middle patch section with

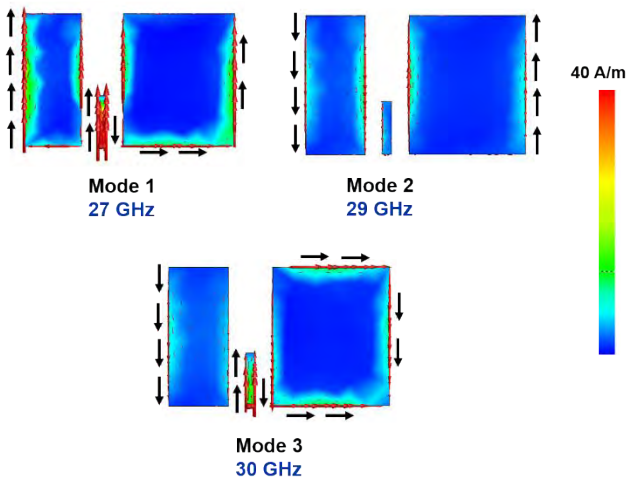

FIGURE 27. Characteristic mode currents of capacitive coupled asymmetric patch structure.

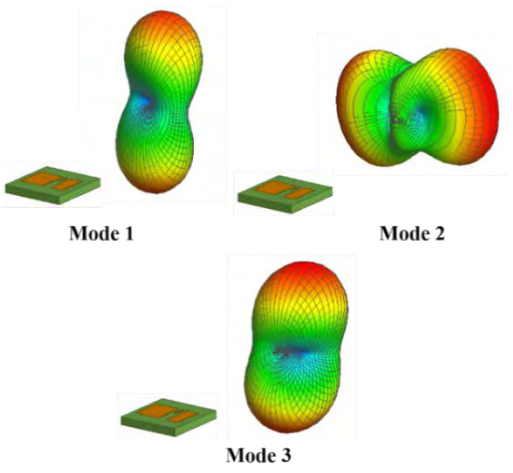

FIGURE 28. Radiation pattern of Eigen modes at resonant frequency.

strong currents in the edges at 30 GHz. The diagonal currents are the strongest when the length of the shorter side of the larger patch becomes comparable to $0.4\lambda_{eff}$. The radiation of this mode is mainly due to the horizontal mode of the patch.

The radiation pattern of each mode at its resonant frequency is shown in Fig. 28. Mode 1 has a broadside pattern with a slight tilt from the broadside direction as the currents in the patches are in phase and the fields add together constructively. The small tilt is due to the weak diagonal currents on the larger patch. In mode 2, the currents on the patches are opposite to each other and hence cancel each other. But since both patches are not symmetric, all the vertical currents are not cancelled out and there is a tilt in the pattern from the antenna axis. Hence there is no radiation in the broadside direction in mode 2. Mode 3 has strong diagonal currents with strong currents in the middle patch section and so the radiation pattern is tilted diagonally from the broadside direction.

For our operation, mode 1 and mode 3 are desired and mode 2 is to be eliminated. Mode 1 and mode 3 can be selected by exciting the structure at maximum mode 1 and mode 3 Eigen current location and mode 2 can be suppressed by placing the feed at weak mode 2 Eigen current location. In this structure, the middle patch section acts as a suitable feed location by exciting mode 1 and mode 3 and suppressing mode 2. There is shift in resonant frequencies from the predicted TCM values upon excitation.

The total current distribution is simulated in CST MWS with the excitation in the small feed patch. The total current distribution of the proposed antenna at 27 GHz with excitation could be deduced as due to mode 1 currents alone as seen in Fig. 29(a). At 30 GHz as seen in Fig. 29(b), the total current distribution with excitation is due to mode 3. Thus the bandwidth gained by the modified structure comes at the expense of the increased size and tilted radiation pattern at higher frequencies around 30 GHz.

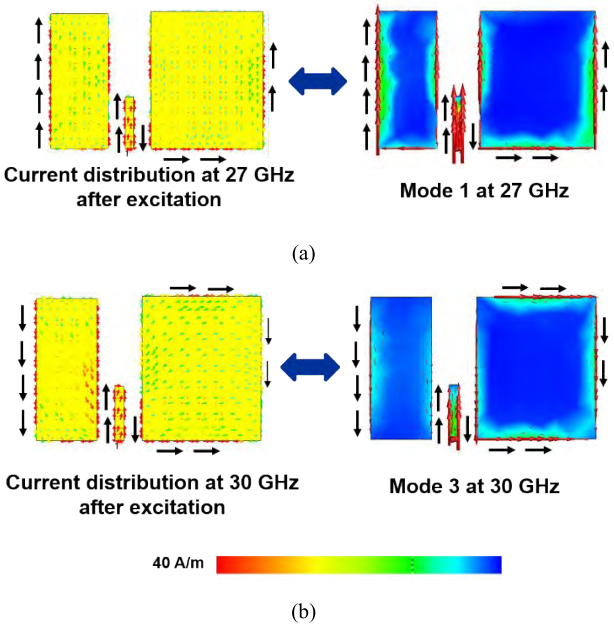

FIGURE 29. Comparison of current distribution after excitation with modal currents at (a) 27 GHz; (b) 30 GHz.

V. STATE OF THE ART COMPARISON

In order to evaluate the achievements of the proposed antenna array with respect to existing designs, the proposed antenna array is compared with recently published designs as shown in Table 1. The key parameters are bandwidth percentage, antenna size, array gain, coverage in the theta plane and the simplicity of antenna structure.

The proposed antenna array provides 360° coverage in the elevation plane. The array provides a minimum gain of 16.5 dBi as the effective antenna aperture and the number of antenna elements are larger. The physical antenna length is relatively small compared with existing designs thereby, consuming less space and hence more antenna elements can

TABLE 1. Comparison of proposed antenna performance with recent antenna designs.

Design	Frequency band(GHz)	Bandwidth (GHz)	Bandwidth (%)	Antenna Size (in mm)	Array Gain (dBi) (8-element)	Coverage (theta plane)	Antenna Structure
[3]	27.4-28.4	1	3.6	4x0.2x1.6	10.5	90^0	Complex Multi-layer
[12]	27-29	2	7.1	5.4x0.6x0.8	11	90^0	Complex Multi-layer
[8]	26-30	4	14.3	-	-	90^0	Complex SIW structure
[11]	21-22	1	4.6	4.32x2x0.8	13.5	270^0	Simple Single-layer
[10]	28-32	4	13.3	4.46x0.2x0.5	12	90^0	Complex SIW structure
Proposed	**24-28**	**4**	**15.4**	**3.25x3.7x0.8**	**16.5 (12-element)**	360^0	**Simple Single-layer**

be arranged along the width of the mobile phone ground plane. The bandwidth of the antenna element is sufficient for 5G smartphone applications and can be further widened by modifying the antenna structure as discussed in Section V. The proposed antenna array is certainly a strong candidate for future 5G mobile phone applications.

VI. CONCLUSION

A novel and compact capacitive coupled symmetric patch antenna has been proposed at mm-Wave frequencies for future 5G smartphone applications. The operating principle of the proposed design has been studied using the equivalent circuit model and Theory of Characteristic Modes. The antenna element covers the frequency range of 24-28 GHz which is a prospective 5G frequency band. Four sub-arrays of 12 antenna elements each providing 90° in the elevation plane have been integrated into the mobile phone chassis for providing 360° coverage. The antenna array achieved a high gain of 16.5 dBi in the boresight and can be steered from −60° to 60° in the phi plane. The proposed antenna exhibited a stable gain and uniform radiation pattern throughout the intended frequency band. The antenna element feeding scheme and the antenna array architecture have been discussed. The antenna array has been fabricated and beam steering performance has been verified for a 1×4 array. Also a modified design to widen the antenna bandwidth has also been studied and presented using the Theory of Characteristic Modes.

REFERENCES

[1] J. G. Andrews *et al.*, "What will 5G be?" *IEEE J. Sel. Areas Commun.*, vol. 32, no. 6, pp. 1065–1082, Jun. 2014.

[2] J. Qiao, X. Shen, J. Mark, Q. Shen, Y. He, and L. Lei, "Enabling device-to-device communications in millimeter-wave 5G cellular networks," *IEEE Commun. Mag.*, vol. 53, no. 1, pp. 209–215, Jan. 2015.

[3] W. Hong, K.-H. Baek, Y. Lee, Y. Kim, and S.-T. Ko, "Study and prototyping of practically large-scale mmWave antenna systems for 5G cellular devices," *IEEE Commun. Mag.*, vol. 52, no. 9, pp. 63–69, Sep. 2014.

[4] J. Helander, K. Zhao, Z. Ying, and D. Sjöberg, "Performance analysis of millimeter-wave phased array antennas in cellular handsets," *IEEE Antennas Wireless Propag. Lett.*, vol. 15, pp. 504–507, Jul. 2015.

[5] H. Zhou, "Phased array for millimeter-wave mobile handset," in *Proc. IEEE Antennas Propag. Soc. Int. Symp.*, Memphis, TN, USA, Jul. 2014, pp. 933–934.

[6] N. Ojaroudiparchin, M. Shen, and G. F. Pedersen, "Multi-layer 5G mobile phone antenna for multi-user MIMO communications," in *Proc. 23rd Telecommun. Forum Telfor*, Belgrade, Serbia, Nov. 2015, pp. 559–562.

[7] D. Psychoudakis, Z. Wang, and F. Aryanfar, "Dipole array for mm-Wave mobile applications," in *Proc. IEEE Antennas Propag. Soc. Int. Symp.*, Orlando, FL, USA, Jul. 2013, pp. 660–661.

[8] H. Zhou and F. Aryanfar, "Millimeter-wave open ended SIW antenna with wide beam coverage," in *Proc. IEEE Antennas Propag. Soc. Int. Symp.*, Orlando, FL, USA, Jul. 2013, pp. 658–659.

[9] Y. Cheon and Y. Kim, "Millimeter-wave phased array antenna with wide beam coverage," in *Proc. Eur. Conf. Antennas Propag.*, Apr. 2016, pp. 1–3.

[10] Q.-L. Yang, Y.-L. Ban, K. Kang, C.-Y.-D. Sim, and G. Wu, "SIW multibeam array for 5G mobile devices," *IEEE Access*, vol. 4, pp. 2788–2796, 2016.

[11] N. Ojaroudiparchin, M. Shen, S. Zhang, and G. F. Pedersen, "A switchable 3-D-coverage-phased array antenna package for 5G mobile terminals," *IEEE Antennas Wireless Propag. Lett.*, vol. 15, pp. 1747–1750, 2016.

[12] N. Ojaroudiparchin, M. Shen, and G. F. Pedersen, "A 28 GHz FR-4 compatible phased array antenna for 5G mobile phone applications," in *Proc. ISAP*, Hobart, TAS, Australia, Nov. 2015, pp. 1–4.

[13] M. Stanley, Y. Huang, T. Loh, Q. Xu, H. Wang, and H. Zhou, "A high gain steerable millimeter-wave antenna array for 5G smartphone applications," in *Proc. Eur. Conf. Antennas Propag.*, Paris, France, Mar. 2017, pp. 1311–1314.

[14] M. Stanley, Y. Huang, H. Wang, H. Zhou, A. Alieldin, and S. Joseph, "A novel mm-Wave phased array antenna with 360° coverage for 5G smartphone applications," in *Proc. 10th UK-Eur.-China Workshop Millimetre Waves Terahertz Technol.*, Liverpool, U.K., Oct. 2017, pp. 1–3.

[15] R. F. Harrington, "Effect of antenna size on gain, bandwidth, and efficiency," *J. Res. Nat. Bur. Standards, D. Radio Propag.*, vol. 64D, no. 1, pp. 1–12, 1960.

[16] C. A. Balanis, *Antenna Theory: Analysis and Design*, 3rd ed. Hoboken, NJ, USA: Wiley, 2005.

[17] R. J. Garbacz and R. Turpin, "A generalized expansion for radiated and scattered fields," *IEEE Trans. Antennas Propag.*, vol. AP-19, no. 3, pp. 348–358, May 1971.

[18] R. F. Harrington and J. R. Mautz, "Theory of characteristic modes for conducting bodies," *IEEE Trans. Antennas Propag.*, vol. AP-19, no. 5, pp. 622–628, Sep. 1971.

[19] W. Hong, K.-H. Baek, and S. Ko, "Millimeter-wave 5G antennas for smartphones: Overview and experimental demonstration," *IEEE Trans. Antennas Propag.*, vol. 65, no. 12, pp. 6250–6261, Dec. 2017.

[20] B. Sadhu, *et al.*, "A 28-GHz 32-element TRX phased-array IC with concurrent dual-polarized operation and orthogonal phase and gain control for 5G communications," *IEEE J. Solid-State Circuits*, vol. 52, no. 12, pp. 3373–3391, Dec. 2017.

[21] B. Yu, K. Yang, C. Y. D. Sim, and G. Yang, "A novel 28 GHz beam steering array for 5G mobile device with metallic casing application," *IEEE Trans. Antennas Propag.*, vol. 66, no. 1, pp. 462–466, Jan. 2018.

[22] X. Yang, Y. Liu, Y.-X. Xu, and S.-X. Gong, "Isolation enhancement in patch antenna array with fractal UC-EBG structure and cross slot," *IEEE Antennas Wireless Propag. Lett.*, vol. 16, pp. 2175–2178, May 2017.

[23] Z. Miers, H. Li, and B. K. Lau, "Design of bandwidth enhanced and multiband MIMO antennas using characteristic modes," *IEEE Antennas Wireless Propag. Lett.*, vol. 12, pp. 1696–1699, Nov. 2013.
[24] J. Kurvinen, A. Lehtovuori, J. Mai, C. Wang, and V. Viikari, "Metal-covered handset with LTE MIMO, Wi-Fi MIMO, and GPS antennas," *Prog. Electromagn. Res. C*, vol. 80, pp. 89–101, Jan. 2018.

MANOJ STANLEY received the B.Tech. degree in electronics and communication from Kerala University, India, in 2012, and the M.Tech. degree in communication systems from the Visvesvaraya National Institute of Technology, India, in 2014. He is currently pursuing the Ph.D. degree in electrical engineering with the University of Liverpool, U.K. He was a Lab Engineer under CoE at the Visvesvaraya National Institute of Technology, where he was involved in projects of national importance. His research interests include mobile phone antenna design, theory of characteristic modes, and MIMO and mm-wave antenna array design for 5G smartphones.

YI HUANG (S'91–M'96–SM'06) received the B.Sc. degree in physics from Wuhan University, China, the M.Sc. (Eng.) degree in microwave engineering from NRIET, Nanjing, China, and the D.Phil. degree in communications from the University of Oxford, Oxford, U.K., in 1994.

He has been conducting research in the areas of wireless communications, applied electromagnetics, radar, and antennas for the past 25 years. He spent three years with NRIET, China, as a Radar Engineer and various periods with the Universities of Birmingham, Oxford, and Essex, U.K., as a Member of Research Staff. He was a Research Fellow with British Telecom Labs in 1994. In 1995, he joined the Department of Electrical Engineering and Electronics, University of Liverpool, U.K., as a Faculty Member, where he is currently a Full Professor in wireless engineering, the Head of the High Frequency Engineering Research Group, the M.Sc. Programme Director, and the Deputy Head of the department. He has published over 200 refereed papers in leading international journals and conference proceedings, and is the principal author of the popular book *Antennas: From Theory to Practice* (Wiley, 2008). He has received many research grants from research councils, government agencies, charity, EU, and industry, acted as a consultant to various companies, and served on a number of national and international technical committees.

Dr. Huang has been a Keynote/Invited Speaker and an Organizer of many conferences and workshops, such as the IEEE iWAT 2010, WiCom 2006, 2010, and LAPC2012. He has been an editor, an associate editor, or a guest editor of four international journals. He is currently the Editor-in-Chief of *Wireless Engineering and Technology*, a U.K. National Representative of European COST-IC1102, an Executive Committee Member of the IET Electromagnetics PN, and a fellow of IET, U.K.

HANYANG WANG (SM'03) received the Ph.D. degree from Heriot-Watt University, Edinburgh, U.K., in 1995. He served as a Lecturer and an Associate Professor with Shandong University, Jinan, China, from 1986 to 1991. From 1995 to 1999, he was a Post-Doctoral Research Fellow with the University of Birmingham, Birmingham, U.K., and the University of Essex, Colchester, U.K. From 1999 to 2000, he was with Vector Fields Ltd., Oxford, U.K., as a Software Development and Microwave Engineering Consultant Engineer. He joined Nokia U.K. Ltd., Farnborough, U.K., in 2001, where he was a Mobile Antenna Specialist for 11 years. He joined Huawei Technology Co., Ltd. after leaving Nokia, and he is currently the Chief Mobile Antenna Expert and the Head of the Mobile Antenna Technology Division. He is also an Adjunct Professor with the School of Electronics and Information Technology, Sichuan University, Chengdu, China. He holds over 40 granted and pending U.S./WO/PCT patents. His current research interests include small antennas for mobile terminals, patch and slotted waveguide antennas and arrays for mobile communications and airborne radars, and numerical methods for the solutions of electromagnetic radiation and scattering problems. He has authored over 80 refereed papers on these topics. He is a Huawei Fellow and an IET/IEE Fellow. He was a recipient of the Title of Nokia Inventor of the Year in 2005 and the Nokia Excellence Award in 2011. He was also a recipient of the Huawei Individual Gold Medal Award in 2012 and the Huawei Team Gold Medal Award in 2013 and 2014, respectively. His patent was ranked number one among 2015 Huawei top ten patent awards. He is an Associate Editor of the IEEE Antennas and Wireless Propagation Letters. He is listed in Marquis Who's Who in the World and the International Biographical Center, Cambridge, U.K.

HAI ZHOU received the Ph.D. degree from the University of London in 1987. He also carried out his post-doctoral research at the University of London until 1992. He served as a Senior Lecturer at South Bank University, London. In 1996, he joined Lucent Technologies and involved in system engineering for 19 years. In 2015, he moved to Huawei Technology Co., Ltd., where he was involved in over-the-air test related standards and 5G antennas. He was involved in various topics from shaped reflector antenna synthesis, FDTD during his academic years to radio resource management, and adaptive antennas in industry. He holds 18 patents. He has authored or co-authored 14 journal papers and 34 conference papers. One of the papers received the Best Paper Award at the 19th European Microwave Conference in 1989 and another received the Oliver Lodge Premium from IEE as the best paper of the year on antennas and propagation in 1991.

AHMED ALIELDIN received the B.Sc. degree in radar engineering from the Military Technical College, Egypt, in 2005, and the M.Sc. (Eng) degree in antenna and microwave propagation from the University of Alexandria, Egypt, in 2013. He was a Radar Engineer under MoD, Egypt, and a Lecturer Assistant with the Air Defence College, Egypt. He was also an Antenna Engineer with Benha Electronics Company, where he was involved in projects of national importance. He is currently pursuing the Ph.D. degree in electrical engineering with the University of Liverpool, U.K. His research interests include mobile base station antennas, satellite antennas, and MIMO and phased-MIMO radar antenna arrays design.

SUMIN JOSEPH received the B.Tech. degree (Hons.) in electronics and communication from the Cochin University of Science and Technology, India, in 2012, and the M.Tech. degree (Hons.) in communication systems from the Visvesvaraya National Institute of Technology, India, in 2015. He is currently pursuing the dual Ph.D. degree in electrical engineering with the University of Liverpool, U.K., and National Tsing Hua University, Taiwan.

He was a Lab Engineer under CoE at the Visvesvaraya National Institute of Technology, where he was involved in projects of national importance. His research interests include self-biased circulators, mm-wave antenna arrays, rectifying antennas, rectifiers, wireless power transfer, and energy harvesting.